Applied Catalysis B: Environmental 92 (2009) 341–350

Contents lists available at ScienceDirect

Applied Catalysis B: Environmental

journal homepage: www.elsevier.com/locate/apcatb

Crystal structure and surface species of $CuFe_2O_4$ spinel catalysts in steam reforming of dimethyl ether

Kajornsak Faungnawakij [a,*], Naohiro Shimoda [b], Tetsuya Fukunaga [c], Ryuji Kikuchi [b], Koichi Eguchi [b,*]

[a] National Nanotechnology Center, National Science and Technology Development Agency, 111 Thailand Science Park, Patumthani 12120, Thailand
[b] Department of Energy and Hydrocarbon Chemistry, Graduate School of Engineering, Kyoto University, Nishikyo-ku, Kyoto 615-8510, Japan
[c] Central Research Laboratories, Idemitsu Kosan Co., Ltd., 1280 Kami-izumi, Chiba 299-0293, Japan

ARTICLE INFO

Article history:
Received 22 April 2009
Received in revised form 18 July 2009
Accepted 11 August 2009
Available online 18 August 2009

Keywords:
Copper–iron spinel
X-ray photoelectron spectroscopy
Auger electron spectroscopy
Methanol
Hydrogen
Regeneration

ABSTRACT

Copper–iron spinel ($CuFe_2O_4$) in cubic phase was prepared via a simple citrate sol–gel method, and was transformed into tetragonal phase of high crystallinity by calcining in air at 900 °C. Composites of $CuFe_2O_4$ spinel and γ-Al_2O_3 were investigated for catalytic production of hydrogen from dimethyl ether steam reforming (DME SR). X-ray photoelectron spectroscopy showed Cu^{1+}-rich surface species (Cu^{1+}/Cu^0 = ca. 3/2 with negligible Cu^{2+}) over the calcined $CuFe_2O_4$ subjected to *in situ* H_2 reduction. The spinel-oxides with lower content of reducible Cu species possessed higher amount of Cu^{1+} species under the reducing atmosphere, corresponding to higher DME SR activity. Copper clusters highly dispersed in the matrix of iron oxides were reduced from the spinel structure, and the strong interaction between them should result in the high activity and durability. The degraded catalysts after DME SR were regenerated by calcining in air in the temperature range of 350–800 °C. Slow deactivation of the composites observed during DME SR at 375 °C was mainly attributable to non-graphitic carbonaceous species deposited on the catalyst surface.

1. Introduction

Spinel-oxides have long played an important role in various catalytic applications, for example, decomposition of gaseous pollutants [1,2] and water gas shift reaction [3,4]. In normal spinels AB_2O_4, *A* is generally a divalent cation occupying tetrahedral sites, while *B* is a trivalent cation occupying octahedral sites. In inverse spinels, half of *B* cations occupy the tetrahedral sites, and the formula is rewritten as $B[AB]O_4$. In recent years, Cu-based spinels have been proposed as a reforming catalyst for hydrogen production from oxygenated hydrocarbons [5–8]. Copper–iron spinel-type oxide ($CuFe_2O_4$) has first been developed as a highly active catalyst for steam reforming of dimethyl ether (DME SR) [6]. Presently, DME is recognized as a promising hydrogen source alternative to liquefied petroleum gas (LPG), methane, and gasoline, since it is harmless and can be reformed at low temperatures of 200–400 °C, producing reformate of a high hydrogen-to-carbon ratio. It has already been used as a clean-burning fuel alternative to LPG and diesel. Although both methanol (MeOH) and DME can be reformed at low temperatures of 200–350 °C for MeOH [9–13] and 200–400 °C for DME [14–19], respectively, DME is non-toxic and thus more preferable to MeOH. These attractive characteristics make DME suitable as a hydrogen carrier for low- and intermediate-temperature fuel cells.

DME SR comprises two moderately endothermic reactions in sequence: hydrolysis of DME and MeOH SR.

$$\text{DME SR}: (CH_3)_2O + 3H_2O_{(g)} \rightarrow 6H_2 + 2CO_2 \quad \Delta H_r^0 = 122\,\text{kJ mol}^{-1} \tag{1}$$

$$\text{DME hydrolysis}: (CH_3)_2O + H_2O_{(g)} \rightarrow 2CH_3OH \quad \Delta H_r^0 = 24\,\text{kJ mol}^{-1} \tag{2}$$

$$\text{MeOH SR}: CH_3OH_{(g)} + H_2O_{(g)} \rightarrow 3H_2 + CO_2 \quad \Delta H_r^0 = 49\,\text{kJ mol}^{-1} \tag{3}$$

Hydrolysis of DME actively takes place over acid catalysts, e.g. zeolite and alumina, while MeOH SR proceeds over Cu- and Pd-based catalysts. As a consequence, a mixture of acid and metal-based catalysts is generally needed for overall DME SR. The Cu-based catalyst is promising in terms of cost effectiveness. The role of acid catalysts was investigated by several researchers [8,17,18]. Ga_2O_3 and Ga_2O_3–Al_2O_3 with and without copper species were

* Corresponding author. Tel.: +81 75 383 2519; fax: +81 75 383 2520.
E-mail addresses: kajornsak@nanotec.or.th (K. Faungnawakij), eguchi@scl.kyoto-u.ac.jp (K. Eguchi).

0926-3373/$ – see front matter © 2009 Elsevier B.V. All rights reserved.
doi:10.1016/j.apcatb.2009.08.013

proposed as an active component for DME SR [16]. We have recently reported the optimum calcination temperature for the composite catalysts of copper–iron spinel and alumina [8,20]. Tanaka et al. studied MeOH SR over Cu-based spinels and reported the oxidation state of copper species characterized by XPS [6]. They reported that both Cu^0 and Cu^{1+} species were expected to contribute to the reaction. The amount of Cu^{1+} surface species over $CuFe_2O_4$ was found to be superior to that over $Cu/ZnO/Al_2O_3$ catalyst, corresponding to their reforming activity [21]. However, the formation mechanisms of the Cu species as well as their contribution to the reaction are not clearly understood yet. Reduction behaviors are anticipated to play a role on the formation of Cu surface species. Moreover, the durability of the composite catalysts under the actual operating conditions is still controversial, which is the most important factor for real applications.

In this study, the activity and durability of $CuFe_2O_4$ spinels mixed with alumina was investigated during DME SR. X-ray photoelectron spectroscopy (XPS) and Auger electron spectroscopy (AES) were conducted to evaluate the characteristics of Cu species in the spinels. Relation between the reducibility of the spinels and the oxidation state of the Cu species was first clarified in the present study. X-ray diffraction analysis was conducted to examine the crystalline phases and crystallite size of the catalysts. Porous structure of the spinels was also evaluated before and after calcination and DME SR.

2. Experimental

2.1. Catalyst preparation

$CuFe_2O_4$ was prepared by a sol–gel combustion method based on citrate complexation as previously described [6,22–24]. The sol–gel combustion combines the chemical sol–gel and the combustion processes and could provide ultrafine powders with large scale production. In this method different cations can effectively be accommodated in the complex, leading to uniform mixing of the cations [25–27]. An aqueous solution of copper and iron nitrates was stirred at 60 °C for 2 h, and then citric acid was added to the solution. The resultant homogeneous solution was then heated to 90 °C to evaporate water. The nitrate–citrate complex gel thus obtained was heated to 140–200 °C to decompose citric acid until fine oxide powders were obtained (referred as *p*-CuFe as-syn). The powders were calcined in air at 900 °C for 10 h (referred as *p*-CuFe 900). The commercially available $CuFe_2O_4$ ($CuFe_2O_4$, BET surface area = 20 $m^2\ g^{-1}$) from Aldrich was used as a reference catalyst. The commercial spinels as-obtained and calcined in air at 900 °C for 10 h were referred as *c*-CuFe as-obt and *c*-CuFe 900, respectively. The DME hydrolysis catalyst was γ-alumina (JRC-ALO-8, hereafter referred to as ALO8) provided by the Catalysis Society of Japan. Additionally, DME SR activity over a commercial catalyst $Cu/ZnO/Al_2O_3$ (Süd-Chemie MDC-3, BET surface area = 72 $m^2\ g^{-1}$), well known as an active MeOH SR catalyst, was tested for comparison. The Cu-based catalyst was mechanically mixed with ALO8 at a fixed weight ratio of 2:1. Before mixing, ALO8 was heat-treated in air at 700 °C for 0.5 h. The mechanical mixture was then pressed, crushed, and sieved to particle sizes of 0.85–1.7 mm.

2.2. Catalyst characterization

XPS coupled with AES was performed using a Shimadzu ESCA-850 with a Mg Kα radiation source ($h\upsilon$ = 1253.6 eV) and operated at 8 kV and 30 mA. When *in situ* XPS/AES analysis was performed, samples were reduced in the internal pre-treatment chamber at 350 °C for 3 h under 10% H_2/N_2 gas flow. Each binding energy was referenced to the C 1s peak (284.3 eV). Powder X-ray diffraction (XRD) patterns were obtained using a Rigaku RINT-2200 with a Cu Kα radiation source (λ = 0.15406 nm) and operated at 40 kV and 40 mA. The crystallite size was calculated by XRD-line broadening using the Scherrer equation. Raman spectra were measured using a JOBIN YVON T64000 equipped with a CCD detector and a 514-nm laser. Scanning electron microscope (SEM) coupled with an energy dispersive X-ray (EDX) was conducted using a Shimadzu SSX-550. Fourier transform infrared (FTIR) spectroscopy was performed using a Jasco FT/IR-410.

Temperature-programmed reduction (TPR) and temperature-programmed oxidation (TPO) were carried out using a CHEMBET-3000. For TPR, a catalyst sample of 25 mg was reduced in 5% H_2/Ar at a flow rate of 30 ml min^{-1} (25 °C, 1 atm) in heating process at a rate of 10 °C min^{-1}. For TPO, a catalyst sample of 50 mg was oxidized in 5% O_2/He at a flow rate of 30 ml min^{-1} (25 °C, 1 atm) in heating process at a rate of 10 °C min^{-1}. The product gases were monitored by an online mass spectrometer. A nitrogen adsorption system (BEL Japan Bellsorp-miniΠ) was employed to determine adsorption–desorption isotherm at liquid nitrogen temperature of −196 °C. The Brunauer–Emmett–Teller (BET) and the Barrett–Joyner–Halenda (BJH) approaches were employed to determine the specific surface area and pore size distribution of the samples, respectively.

2.3. Catalyst activity-durability evaluation

Catalytic activity was evaluated in a conventional flow reactor under atmospheric pressure. Reaction tests were carried out over catalyst samples without pre-reduction process. Unless otherwise stated, a mixture of steam and DME at a steam-to-carbon ratio (S/C) of 2.5 (25 °C, 1 atm) was supplied through mass flow controllers to a pre-heater at 150 °C, and then to the catalyst bed at the designated reaction temperature. The catalyst bed temperature was raised from 250 to 375 °C at a heating rate of 2.5 °C min^{-1}, and gas analysis was performed from 250 °C at a constant interval of 25 °C. The catalyst bed temperature was kept constant at each reaction temperature for 1 h prior to gas analysis. After the temperature reached final set temperature of 375 °C, it was kept constant for ca. 50 h and the gas analysis was periodically carried out. All reacted catalysts were exposed to air after cooled down to room temperature in N_2 flow. Although the reaction temperature was controlled carefully, small fluctuation at ca. 0–6 °C below the setting temperature, depending on degree of the SR reaction, occurred due to the endothermic nature of the related reactions. Compositions of the influent and effluent gas were analyzed with online gas chromatographs equipped with FID (Shimadzu, GC-9A) and TCD (VARIAN, CP-4900). The steam in the feed and reformate was trapped by a condenser at ca. 3 °C before the gas analysis. A Poraplot U column was used for separation of DME, MeOH, and CO_2, and a molecular sieve 5A column was for separation of H_2, N_2, CH_4, and CO. DME conversion and selectivity to C_1 species are defined as follows:

$$\text{DME conversion}\ (\%) = 100\left(\frac{F_{CO} + F_{CO_2} + F_{CH_4}}{F_{CO} + F_{CO_2} + F_{CH_4} + 2F_{DME}}\right) \quad (4)$$

$$\text{Selectivity to } C_1 \text{ species} = 100F_{C_1} / \sum F_{C_1} \quad (5)$$

where F_{DME} and F_{C_1} is the molar flow rate of DME and C_1-containing products such as CH_4, CO, and CO_2 in the effluent gas, respectively. Note that the conversion defined here can be deviated from an actual value when solid carbonaceous species were significantly formed. All experiments conducted showed a carbon balance above 97% with a negligible amount of MeOH and higher carbon-containing gaseous products, and consequently solid carbon species were eliminated from the calculation. Deactivation

of catalyst at reaction time t (D_t) was expressed in Eq. (6), which was defined as a ratio of DME conversion at reaction time of t h referred to that of 1 h. Hydrogen yield was defined by Eq. (7) as a ratio of experimental and theoretical mole of hydrogen produced per mole of DME in the feed gas.

$$\text{Deactivation } D_t\,(\%) = 100\left(1 - \frac{\text{DME conversion at } t\text{ h}}{\text{DME conversion at 1 h}}\right) \quad (6)$$

$$\text{H}_2\text{ yield}\,(\%) = 100\frac{F_{\text{H}_2}}{F_{\text{DME in}}}x\left(\frac{F_{\text{DME in}}}{F_{\text{H}_2}}\right)_T \quad (7)$$

where F_{H_2} and $F_{\text{DME in}}$ are the molar flow rate of H_2 in effluent and DME in feed, respectively. $\left(\frac{F_{\text{DME in}}}{F_{\text{H}_2}}\right)_T = \left(\frac{1}{6}\right)$ is the theoretical molar ratio of DME fed and H_2 produced (see Eq. (1)).

3. Results and discussion

3.1. Catalytic activity and durability

In the reaction tests, a high reforming temperature of 375 °C and high GHSV of 9100 h^{-1} were intentionally adopted as an accelerating condition for deactivation of the Cu catalyst, so that changes in DME conversion could definitely be observed. Fig. 1 illustrates (a) temperature profile of DME conversion in the temperature range from 250 to 375 °C as well as (b) DME conversion at 375 °C with time-on-stream over the composite catalysts. The calcined catalysts, *p*-CuFe 900 + Al_2O_3 and *c*-CuFe 900 + Al_2O_3 showed markedly higher activity than the *p*-CuFe as-syn + Al_2O_3 and *c*-CuFe as-obt + Al_2O_3. In Fig. 1b, over the calcined samples, DME conversion gradually decreased in 55 h from ca. 65 to 60% for *p*-CuFe 900 + Al_2O_3 and from ca. 60 to 55% for *c*-CuFe 900 + Al_2O_3. Fast degradation in the catalytic activity of *p*-CuFe as-syn was observed, while *c*-CuFe as-obt was essentially stable at low conversion.

Table 1 represents DME conversion, product selectivity, H_2 yield and deactivation of composite catalysts as well as thermodynamic equilibrium of DME SR and DME hydrolysis at various reaction conditions. The equilibrium composition was calculated by Gibbs free energy minimization with constraints of no methane or carbon formation. A complete conversion of DME was achieved at GHSV below 2000 h^{-1} and temperature range of 375–400 °C, with negligible deactivation. Concentration of H_2, CO, and CH_4 was 71–73%, 2–3%, and 0.02–0.50%, respectively. Under these conditions, concentration of all products agreed fairly well with the equilibrium. Selectivity to H_2 and CO_2 was slightly greater than that at the equilibrium, while CO selectivity was lower. Concentration of CO was always below or equal to its equilibrium one. The results confirmed that CO was produced from reverse water gas shift reaction (r-WGSR) following the direct formation of H_2 and CO_2 via MeOH SR, though some reports proposed the reaction sequence of MeOH SR was MeOH decomposition followed by water gas shift reaction [28]. Methane was scarcely detected at below 1% on dry basis.

Effect of S/C ratio over *p*-CuFe 900 + Al_2O_3 was evaluated by varying S/C from 1.5 to 2.5. As also shown in Table 1, at S/C = 1.5 (the stoichiometric ratio of DME SR) DME conversion was obtained at 57%, and the increase in S/C from 1.5 to 2.0 and 2.5 markedly raised DME conversion to 62% and 67%, respectively, because DME hydrolysis was promoted. Since DME hydrolysis is controlled by thermodynamic equilibrium, DME hydrolysis (Reaction (2)) can be shifted in the forward direction by increasing S/C or temperature, resulting in a high overall conversion. In addition, fast MeOH SR rate would also shift DME hydrolysis towards the products. A close contact of alumina and copper is favorable for DME SR. It is known that reaction rate of DME hydrolysis over alumina is much slower than that of MeOH SR over Cu catalyst, and therefore DME hydrolysis is considered a rate-determining step [7,9]. Deactivation (D_{10}) of the catalyst at S/C of 1.5 was obviously higher than that at S/C of 2.5. The influence of S/C ratios on degradation behavior suggested that carbonaceous deposition was a reason for the catalyst deactivation. It is generally acceptable that the higher steam content would inhibit carbon formation through reactions of carbon-related species such as DME, MeOH, CO, and CH_4. Thermodynamic equilibrium calculation also confirmed that coke formation could be inhibited by increasing S/C. Additionally, the higher steam contents could attenuate CH_4 and CO formation since DME decomposition and r-WGSR were suppressed.

$$\text{DME decomposition}: (CH_3)_2O \rightarrow CH_4 + CO + H_2 \quad \Delta H_r^0 = -1\text{ kJ mol}^{-1} \quad (8)$$

$$\text{r-WGSR}: CO_2 + H_2 \rightarrow H_2O_{(g)} + CO \quad \Delta H_r^0 = 41\text{ kJ mol}^{-1} \quad (9)$$

In comparison, $Cu/ZnO/Al_2O_3$ mixed with alumina showed relatively low DME SR even at low GHSV of 2000 h^{-1}. Severe decline in the activity was observed due to fast Cu sintering at 375 °C. Methanation was highly selective according to the high alumina content.

Deactivation behavior was investigated by treating the composite catalysts under various atmospheres prior to DME SR. Fig. 2 represents DME conversion and H_2 production rate over *p*-

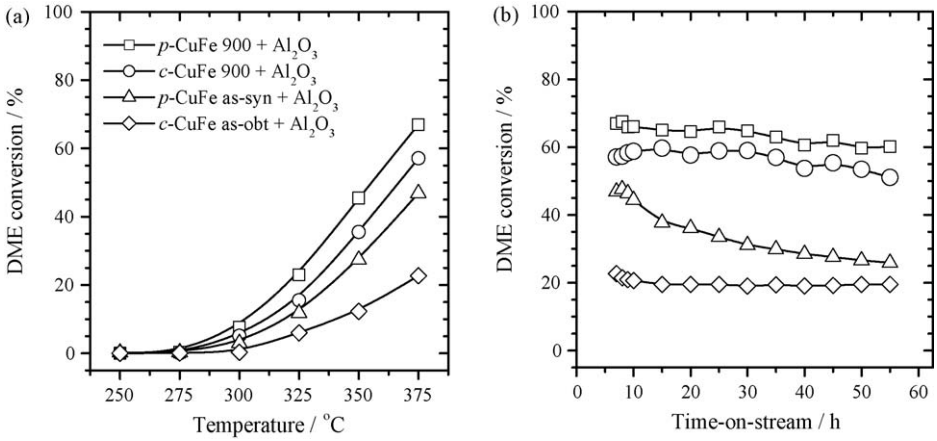

Fig. 1. DME SR over spinel-alumina composite catalysts: (a) temperature dependence and (b) time dependence at constant temperature of 375 °C. Reaction conditions: S/C = 2.5; GHSV = 9100 h^{-1}.

Table 1
Catalytic performance of *p*-CuFe 900 + Al_2O_3 and Cu/ZnO/Al_2O_3 + Al_2O_3 and thermodynamic equilibrium data.

Catalyst	Reforming condition			Deactivation			DME conversion[b]	Selectivity to products and H_2 yield[b]			
	S/C	Temperature (°C)	GHSV (h^{-1})	D_{10} (%)	D_{50} (%)	D_{100} (%)	(%)	CH_4 (%)	CO (%)	CO_2 (%)	H_2 yield (%)
p-CuFe 900 + Al_2O_3	1.5	375	6200	6.4	–	–	56.8	0.6	11.7	87.7	48.0
	2.0	375	7500	6.2	–	–	61.9	0.3	10.5	89.2	53.5
	2.5	375	9100	2.9	9.9	–	67.0	0.1	9.0	90.9	57.0
	2.5	375	3000	0.8	2.8	4.1	93.7	0.1	13.9	86.0	81.6
	2.5	375	2000	0.1	1.6	1.7	99.6	0.1	13.5	85.4	97.6
	2.5	390	2000	0.3	0.2	0.5	100	1.2	11.0	87.8	96.8
Cu/ZnO/Al_2O_3 + Al_2O_3	2.5	375	2000	10.1	20.6		55.9	2.6	13.9	83.5	46.6
Equilibrium of DME SR[a]	2.5	375	–	0	0		100	0	13.6	86.4	95.5
Equilibrium of DME hydrolysis	1.5	375	–	0	0		28.1	0	0	0	0
	2.5	375	–	0	0		34.9	0	0	0	0

[a] Determined by Gibbs free energy minimization with constraints of no CH_4 or coke formation.
[b] The value at time-on-stream of 1 h.

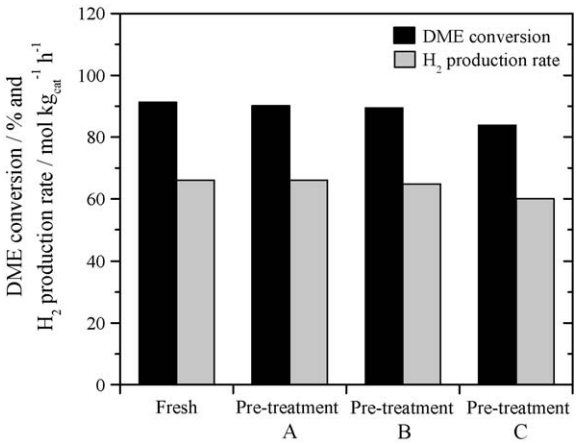

Fig. 2. Pre-treatment effect on DME conversion and hydrogen production rate over *p*-CuFe 900 + Al_2O_3. Reaction conditions: S/C = 2.5; GHSV = 2000 h^{-1}; temperature = 350 °C. Pre-treatment conditions: A = reduction in 10% H_2/N_2 at 350 °C for 3 h, B = A followed by thermal treatment in N_2 at 350 °C for 100 h, C = A followed by steam treatment in 70% H_2O/N_2 at 350 °C for 100 h.

CuFe 900 + Al_2O_3 at reaction temperature of 350 °C with various pre-treatment conditions. The catalytic activity of the sample pre-reduced at 350 °C in 10% H_2/N_2 for 3 h was comparable to that of the fresh catalyst. The activity was unchanged when the pre-reduced catalyst pre-treated at 350 °C in N_2 atmosphere for 100 h. However, when the pre-reduced catalyst was further treated at 350 °C in 70% H_2O/N_2 for 100 h, obvious decline in the activity was observed. These results suggested that steam gave an undesirable effect on catalytic reforming activity, while heat treatment in N_2 and reduction in H_2/N_2 atmosphere had an insignificant impact on the activity.

3.2. Regeneration

Regeneration of spent catalysts was studied by post-reduction and post-calcination processes. As shown in Fig. 3, only 1–2% of the catalytic activity of spent catalyst could be recovered by reduction in 10% H_2/N_2 at 350 °C for 5 h, indicating that oxidation of Cu would not be a main reason for the deactivation. The same catalyst was further calcined in air at 350 °C for 5 h. As a result, a recovery of the DME SR activity was achieved. The recovery of degraded catalysts

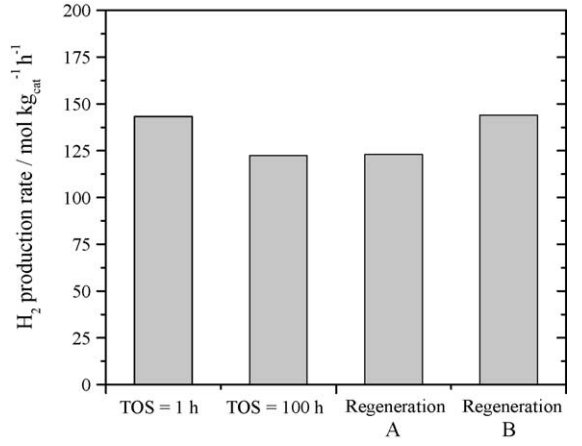

Fig. 3. Post-treatment effect on hydrogen production rate over *p*-CuFe 900 + Al_2O_3. Reaction conditions: S/C = 2.5; GHSV = 3000 h^{-1}; temperature = 375 °C. Regeneration conditions: A = reduction in 10% H_2/N_2 at 350 °C for 5 h, B = calcination in air at 350 °C for 5 h.

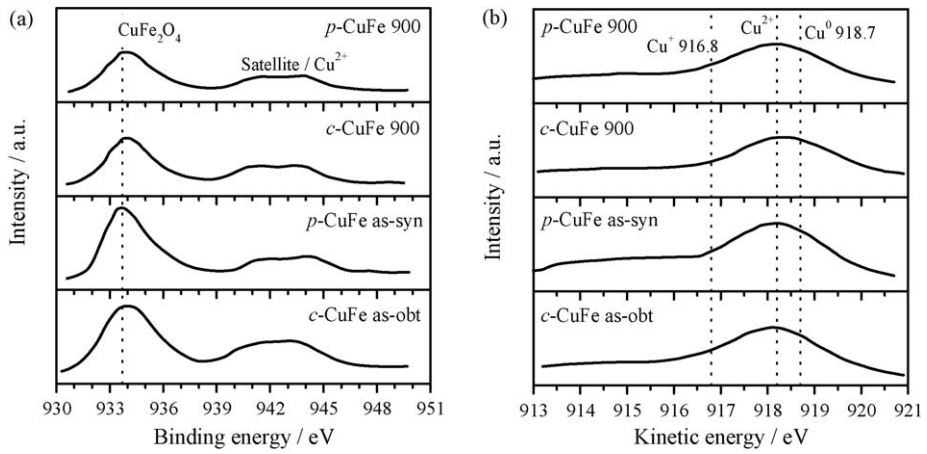

Fig. 4. (a) Cu $2p_{3/2}$ XPS spectra and (b) Cu LMM Auger spectra of spinels *c*-CuFe as-obt, *p*-CuFe as-syn, *c*-CuFe 900, and *p*-CuFe 900.

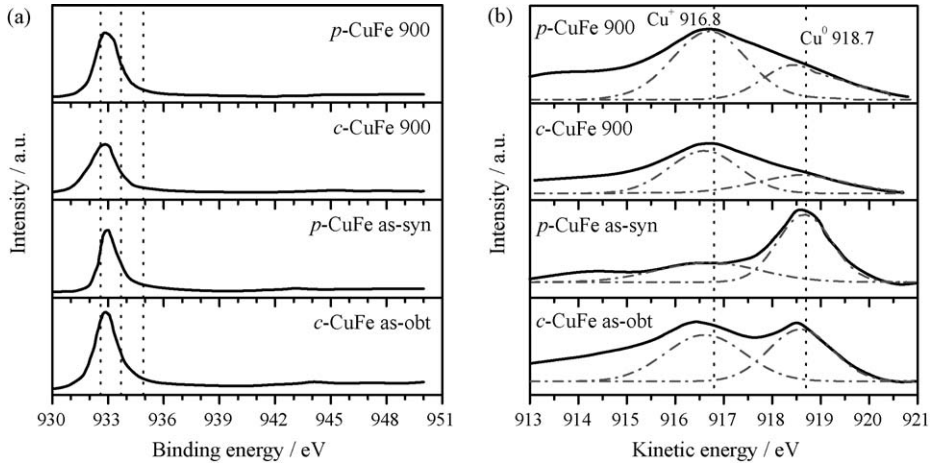

Fig. 5. (a) Cu $2p_{3/2}$ XPS spectra and (b) Cu LMM Auger spectra of *in situ* reduced spinels; *c*-CuFe as-obt, *p*-CuFe as-syn, *c*-CuFe 900, and *p*-CuFe 900. *In situ* reduction conditions: 10% H_2/N_2 at 350 °C for 3 h.

could also be achieved at the calcination temperature up to 800 °C (result not shown). Note that the degraded catalyst could be fully re-activated by such oxidation treatment without post-reduction. Regeneration of commercial $Cu/ZnO/Al_2O_3$ catalysts by calcination may not be possible because of sintering of copper species at high temperatures above 300 °C [29]. The calcination treatment was known as an effective technique to burn out carbonaceous species deposited on catalyst surfaces. At this stage, carbonaceous deposition and/or Cu sintering were considered as the main reasons of the deactivation. The mechanism of deactivation and

Table 2
Peak characteristics and composition ratio of the zero- and monovalent copper from Cu $2p_{3/2}$ and Cu LMM spectra over spinel catalysts together with the characteristics of CuO, metallic Cu, Cu_2O, and $Cu(OH)_2$.

Catalyst	Cu $2p_{3/2}$		Cu LMM					
	Binding energy (eV)		Kinetic energy (eV)			Composition (%)		
	Main peak	Satellite	Cu^0	Cu^{1+}	Cu^{2+}	Cu^0	Cu^{1+}	Cu^{2+}
p-CuFe 900	933.9	d[a]	n/d	n/d	918.2	n/c[c]	n/c	n/c
p-CuFe 900 (*in situ* reduced)	932.7	n/d[b]	918.5	916.7	n/d	30.5	69.5	–
c-CuFe 900	933.9	d	n/d	n/d	918.3	n/c	n/c	n/c
c-CuFe 900 (*in situ* reduced)	932.7	n/d	918.4	916.7	n/d	31.3	68.7	–
p-CuFe as-syn	933.7	d	n/d	n/d	918.1	n/c	n/c	n/c
p-CuFe as-syn (*in situ* reduced)	933.0	n/d	918.7	916.7	n/d	64.4	35.6	–
c-CuFe as-obt	933.9	d	n/d	n/d	918.2	n/c	n/c	n/c
c-CuFe as-obt (*in situ* reduced)	932.9	n/d	918.6	916.6	n/d	47.5	52.5	–
Cu_2O[d]	932.6	n/d	–	916.8	–	–	–	–
Metallic copper[d]	932.67	n/d	918.65	–	–	–	–	–
CuO	933.7	d	–	–	917.7	–	–	–
$Cu(OH)_2$	934.8	d	–	–	916.7	–	–	–

[a] Detected.
[b] Not detected.
[c] Not calculated.
[d] Data taken from literatures [24–26].

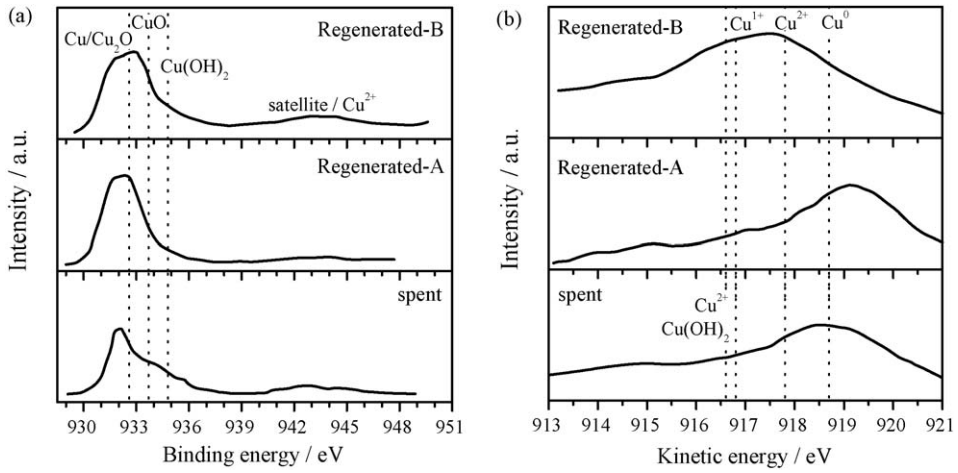

Fig. 6. (a) Cu $2p_{3/2}$ XPS spectra and (b) Cu LMM Auger spectra of spent and regenerated composites of *p*-CuFe 900 + Al_2O_3. Reaction conditions: S/C = 2.5; GHSV = 3000 h^{-1}; temperature = 375 °C; TOS = 100 h. Regeneration conditions: A = reduction in 10% H_2/N_2 at 350 °C for 5 h, B = calcination in air at 350 °C for 5 h.

regeneration was investigated and will be discussed in the latter sections.

3.3. XPS and AES characteristics

Oxidation state of elements was determined for Cu spinels by XPS coupled with AES. Fig. 4 shows Cu $2p_{3/2}$ (930–950 eV) and Cu LMM (912–921 eV) spectra of $CuFe_2O_4$ spinels. In Fig. 4a, the satellite peak of Cu^{2+} species was observed at 937–950 eV for all samples. The main peaks of *p*-CuFe as-syn, *p*-CuFe 900, *c*-CuFe as-obt and *c*-CuFe 900 were 933.7, 933.9, 933.9, and 933.9 eV, respectively. The peak position was in line with the Cu^{2+} species (CuO) peak at 933.7 eV. Cu LMM spectra of all samples exhibited a single peak at ca. 918.1–918.3 eV, which should be assignable to a characteristic peak for Cu^{2+} species.

In situ reduction of the spinels was carried out to evaluate the active species for DME SR reaction. Fig. 5 shows (a) Cu $2p_{3/2}$ and (b) Cu LMM spectra of the samples reduced in 10% H_2/N_2 at 350 °C for 3 h. In the Cu $2p_{3/2}$ spectra, the satellite peak was not detectable, indicating that the divalent copper species in the spinel was completely reduced and the copper species could be zero- or monovalent. The valences were further distinguished by Cu LMM spectra shown in Fig. 5b. Table 2 summarizes the peak characteristics and composition ratio of the zero- and monovalent copper determined from Cu $2p_{3/2}$ and Cu LMM spectra. The characteristics of CuO, metallic Cu, Cu_2O, and $Cu(OH)_2$ were also added in the table. In Fig. 5b, two main peaks were observed for all samples at ca. 916.8 (Cu^{1+}) and 918.7 eV (Cu^0) with different composition ratios. The high proportion of Cu^{1+} species of 69.5% and 68.7% was observed for *p*-CuFe 900 and *c*-CuFe 900, respectively. The *p*-CuFe as-syn and *c*-CuFe as-obt possessed moderate and low proportion of Cu^{1+} at 52.5% and 35.6%, respectively. In Fig. 5a, the Cu $2p_{3/2}$ of the calcined spinels shifted to the lower binding energy, indicating the Cu^{1+}-rich surface.

Fig. 6 shows (a) Cu $2p_{3/2}$ and (b) Cu LMM spectra of spent and regenerated composites of *p*-CuFe 900 + Al_2O_3. The reaction and regeneration conditions used here were the same as in Fig. 3. The small satellite peak was detected over the spent catalyst, indicating the presence of Cu^{2+} species which should be mainly ascribed to CuO. Cu LMM spectra revealed that the Cu^0 was a main component with a small level of Cu^{2+} (CuO), while Cu^{2+} ($Cu(OH)_2$) was negligible. It is considered that Cu surface could be oxidized and then formed Cu^0 and Cu^{1+} simultaneously during the reforming reaction. Steam is generally acceptable as an oxygen source for oxidation of Cu, while H_2 along with CO is a reducing agent of oxidized Cu species. The kinetic reaction scheme of MeOH SR taking place over the Cu species was proposed by several researchers [30,31], and was represented as follows:

$$2CH_3OH \rightarrow CH_3OCHO + 2H_2 \quad (10)$$

$$CH_3OCHO + H_2O \rightarrow HCOOH + CH_3OH \quad (11)$$

$$HCOOH \rightarrow CO_2 + H_2 \quad (12)$$

The mildly oxidized copper species would co-exist with metallic copper, and the high catalytic activity should be attributed to the higher content of Cu^{1+} species of the spinels. It is known that the Cu^0/Cu^{1+} ratio would determine the formation of intermediates during the overall reforming process and should be involved with the reducibility (redox reversibility) of catalysts. It was suggested that a Cu^{1+}/Cu^0 ratio on the surface controlled the catalytic activity for methanol synthesis [32]. It was reported that CH_3OH was oxidized to CH_3O (an intermediate in Reaction (10)) on Cu^0-rich surface, while on Cu^{1+}-rich surface the initially formed CH_3O was further oxidized to formate ion (an intermediate in Reaction (11)) [33]. As reported by Jiang et al. [34], the hydrogen extraction from adsorbed methoxy groups was rate-determining to the overall

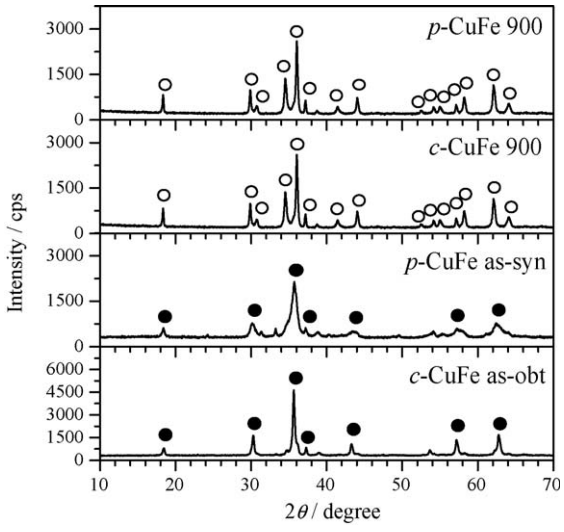

Fig. 7. XRD patterns of spinels *c*-CuFe as-obt, *p*-CuFe as-syn, *c*-CuFe 900, and *p*-CuFe 900. $CuFe_2O_4$ tetragonal (○), $CuFe_2O_4$ cubic (●).

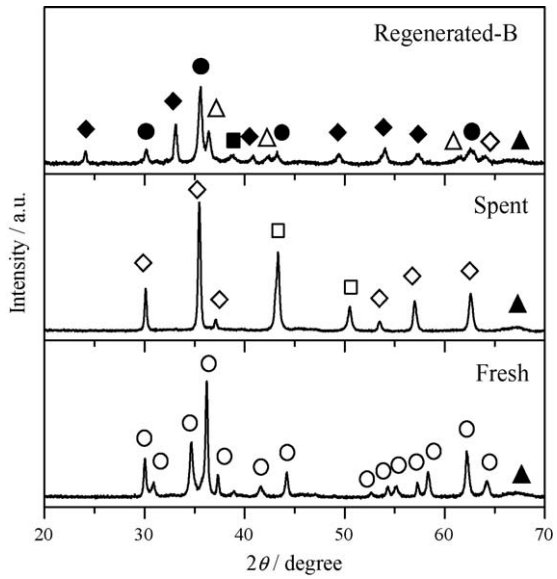

Fig. 8. XRD patterns of *p*-CuFe 900 + Al_2O_3 composite catalysts before and after reaction and regeneration. Reaction conditions: same as in Fig. 6. Regeneration condition: B = calcination in air at 350 °C for 5 h. $CuFe_2O_4$ tetragonal (○), $CuFe_2O_4$ cubic (●), Fe_3O_4 (◇), Fe_2O_3 (◆), Cu (□), CuO (■), Cu_2O (△), Al_2O_3 (▲).

MeOH SR processes. It should be noted that the state of copper in the working condition in the presence of DME and H_2O as well as reaction intermediate and gaseous reformate species would be complicated and different from the reduced samples. Concerning the regenerated catalysts, no significant change in XPS spectra after post-reduction process at 350 °C for 5 h in 10% H_2/N_2 was observed. When the spent catalyst was post-treated by calcination in air at 350 °C for 5 h, Cu^{1+} and Cu^{2+} species appeared, and Cu^0 species disappeared correspondingly.

It can be considered that the oxidation state of Cu species from spinel would remain considerably stable since the catalytic activity of catalysts remained highly stable. The reductive degradation by reducing species formed in the reaction might occur if the reaction time is largely prolonged. It was reported that fast deactivation of $Cu/ZnO/Al_2O_3$ was observed at an initial operation of MeOH SR due to the change in oxidation state of Cu [35]. Ilinich et al. [36] proposed the deactivation mechanism of $Cu–Al_2O_3–CuAl_2O_3$ under the simulated reformate gas. After reaction with steam, the copper oxide crystallites were covered with the dense shell of hydrogen-bonded surface hydroxides. However, since the activity was not recovered largely after post-reduction at 350 °C as mentioned above, the oxidation effect by steam can not be a main reason for the activity decline over the catalyst. The absence of copper hydroxides on the spent catalysts was confirmed by Raman spectroscopy (result not shown). Raman spectra revealed that the bands at 503 and 600 cm^{-1} which are associated with $Cu(OH)_2$ and/or CuOH species were not observed. Not only the surface species but also the interaction between the copper species and the supports or surrounding matrix, crystallinity, and reducibility of the copper species would influence the activity of the catalysts.

3.4. XRD, TPO, and TPR characteristics

XRD patterns of $CuFe_2O_4$ spinels are shown in Fig. 7. The *p*-CuFe as-syn and *c*-CuFe as-obt were identified as a cubic spinel. The high intensity of *c*-CuFe as-obt indicated the great crystallinity of the commercial $CuFe_2O_4$. After calcination in air at 900 °C, the cubic phase was transformed to tetragonal phase and the crystallinity of both calcined spinels became almost the same. A single phase of tetragonal spinel was formed without decomposition to other crystalline phases. Generally, the crystal structure of spinels can be formed as cubic or tetragonal. As for $CuFe_2O_4$, the cubic-to-tetragonal phase transformation of $CuFe_2O_4$ is irreversible since the tetragonal distortion of $CuFe_2O_4$ is more thermodynamically stable than the cubic one. Similar behavior of the temperature-induced phase transition was studied for Cu–Mn spinel [37]. Crystallite size and crystalline phase of the $CuFe_2O_4$ spinels as well as BET surface area, and total pore volume are given in Table 3. The crystallite size of *p*-CuFe as-syn was ca. 12 nm, while that of the other spinels was ca. 40–45 nm. XRD patterns of fresh, spent, and regenerated composite catalysts are shown in Fig. 8. All spent catalysts consisted of three main phases of metallic Cu, Fe_3O_4, and γ-Al_2O_3. Note that the other Cu species could exist in an amorphous state or just on the surface, and therefore could not be detected by XRD. The easily oxidized state corresponds to amorphous copper, while the hardly oxidized state consists of crystalline copper [38]. The active phase for MeOH SR was mainly assigned to the metallic Cu that could act as zero-, mono-, and/or divalences during the reactions. The crystallite sizes of the metallic copper in Al_2O_3-mixed *p*-CuFe as-syn, *p*-CuFe 900, *c*-CuFe as-obt, and *c*-CuFe 900 were 41.4, 36.2, 37.2, and 26.7 nm, respectively. The Cu sizes of the developed and the commercial catalysts were nearly comparable. Focusing on the *p*-CuFe 900 + Al_2O_3, the sizes of Cu after DME SR reaction at 375 °C for 10, 55, and 100 h were 36.4, 36.2, and 37.2 nm, respectively. These results suggested that Cu sintering was unobvious, and therefore would not degrade the catalyst.

Next, the spent catalysts after the reaction test for 100 h were regenerated by calcination in air at 350 °C, and XRD pattern of the regenerated catalysts was measured. From the XRD patterns, it was confirmed that the regenerated catalysts were composed of the mixed oxides of cubic $CuFe_2O_4$, Fe_2O_3, CuO, Cu_2O, and Al_2O_3, indicating that Cu spinel was partially reformed by the calcination of the spent catalysts in air at 350 °C. No evidence of sintering of copper species in the present catalyst was observed, although a usual sintering of copper is generally found in Cu/ZnO and $Cu/ZnO/Al_2O_3$ under the same calcination condition. The high sintering resistivity should be ascribable to the regeneration of spinel accompanied with the high dispersion of Cu in the matrix of iron oxides and their strong interaction. Note that no change in the XRD pattern was observed after post-reduction process. The high dispersion of Cu nanoclusters in the matrix of iron oxides reduced form the spinel structure effectively stabilizes copper and prevents

Table 3
BET surface area, pore volume, crystalline phase, and crystallite size of Cu spinels and alumina.

Catalyst	BET surface area ($m^2 g^{-1}$)	Pore volume ($ml g^{-1}$)	Crystalline phase (–)	Crystallite size[a] (nm)
p-CuFe 900	0.5	0.001	$CuFe_2O_4$ tetragonal	45.0
c-CuFe 900	1.8	0.005	$CuFe_2O_4$ tetragonal	40.5
p-CuFe as-syn	29.3	0.139	$CuFe_2O_4$ cubic	12.5
c-CuFe as-obt	21.0	0.068	$CuFe_2O_4$ cubic	40.5
ALO8	141.0	1.180	γ-Al_2O_3	n/c[b]

[a] Determined from the spinel peaks at 2θ of 36.0° (tetragonal) and 35.7° (cubic) based on the Scherrer equation.
[b] Not calculated.

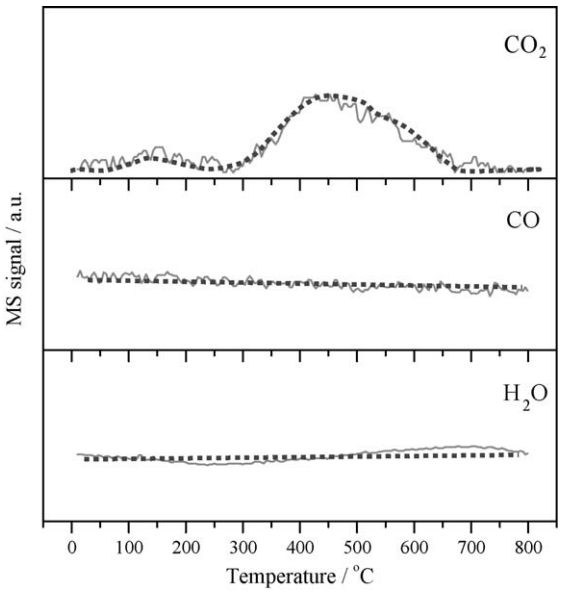

Fig. 9. Desorption curve of CO_2, CO, and H_2O during TPO from the spent *p*-CuFe 900 + Al_2O_3. Reaction conditions: same as in Fig. 6. TPO conditions: 10 °C min^{-1} in 5% O_2/He. Dotted lines represent the smoothing curves.

crystallite growth even at a high temperature of 375 °C, which is a severe condition for sintering of metallic Cu in conventional Cu-based catalysts. There are no graphitic carbon peaks (2θ = 26.3°, 45.2°, 53.9°, and 77.0°) observed by XRD, indicating that the carbon content should be extremely low or it stayed in an amorphous form. Raman spectroscopy analysis confirmed the absence of the graphitic carbon bands at 1343 and 1584 cm^{-1} (result not shown). DME as well as MeOH has no C–C bonds, hence minimizing coking and leading to low reforming temperatures of 200–400 °C. However, the carbon can also be formed through other carbon-containing sources. Based on thermodynamic analysis, the reaction conditions of DME SR at S/C of 2.5 and reaction temperatures of 200–400 °C are in the carbon formation region; the temperature required for coke-free condition is at least 600 °C that is too severe for copper catalyst [39].

Fig. 9 shows the desorption curve of CO_2, CO, and H_2O measured by mass spectrometry (MS) during TPO analysis of the spent composite catalyst of *p*-CuFe 900 + Al_2O_3. The signal for CO_2 evolution was clearly observed in the temperature range of 300–650 °C. Production of CO and H_2O was negligible through the oxidation temperature range studied. It is generally known that the carbonaceous deposits can be removed via calcination in air or oxygen. As shown in the regeneration section, the degraded catalyst can be fully recovered by calcination in air at the temperature range of 350–800 °C, which is consistent well with the TPO analysis. Several attempts were employed to figure out the deposited species. Formates and carbonates are known as deactivators of a WGSR catalyst. However, no evidence for such species on the spent catalysts was obtained in FTIR spectra. By SEM observation coupled with EDX analysis, adsorbed carbon species was not clearly perceived on the catalyst surface. These analyses confirmed that non-graphitic carbon deposition rate on the developed catalysts was considerably slow. Even if coking is favorable and deactivates the catalyst, an effective regeneration by calcination in air at the temperature range of 350–800 °C can be feasible.

Fig. 10a shows the TPR profiles of *p*-CuFe as-syn, *p*-CuFe 900, *c*-CuFe as-obt, and *c*-CuFe 900. The first reduction of all spinels appearing at lower temperature should be assigned to the reduction of spinel ($CuFe_2O_4 \rightarrow Cu + Fe_2O_3$), while the hematite Fe_2O_3 was rapidly reduced to magnetite Fe_3O_4. The reduction peaks at above 400–450 °C should be ascribable to the reduction of Fe_3O_4 to metallic iron. The reduction peaks of spinel and iron oxides shifted to the higher reduction temperatures after calcination at 900 °C, indicating lower content of reducible species and therefore lower reducibility. In comparison between the calcined spinels, hydrogen consumption over *p*-CuFe 900 for reduction of copper species (first peak) was larger than that over *c*-CuFe 900, suggesting that *p*-CuFe 900 contained less reducible copper species. The reducibility of the spinel should influence the copper state under the working condition. By comparing the Cu^{1+}/Cu^0 ratio and the reducibility, the lower content of reducible Cu species corresponds to the higher content of Cu^{1+} species in reduced catalysts. Fig. 10b depicts TPR profiles of the spent *p*-CuFe 900 + A_2O_3. No significant peak was observed up to the reduction temperature of 375 °C that is equal to the reaction temperature, except a small reduction peak at 180–250 °C that should be ascribable to oxidized Cu species.

3.5. BET surface area and BJH pore size analyses

BET surface area of the present spinel catalyst drastically decreased from 29.3 to 0.5 $m^2\ g^{-1}$ after calcination at 900 °C due

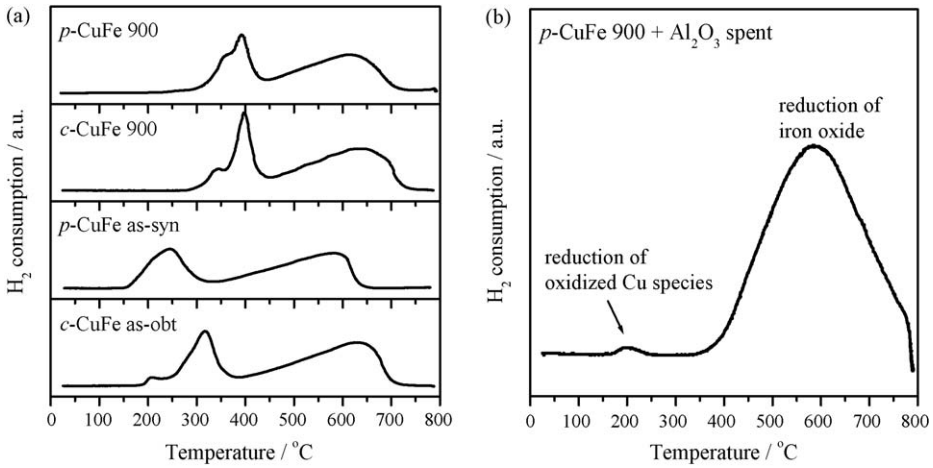

Fig. 10. TPR profiles of (a) *c*-CuFe as-obt, *p*-CuFe as-syn, *c*-CuFe 900, *p*-CuFe 900 and (b) the spent *p*-CuFe 900 + Al_2O_3. Reaction conditions: same as in Fig. 6. TPR conditions: 10 °C min^{-1} in 5% H_2/Ar.

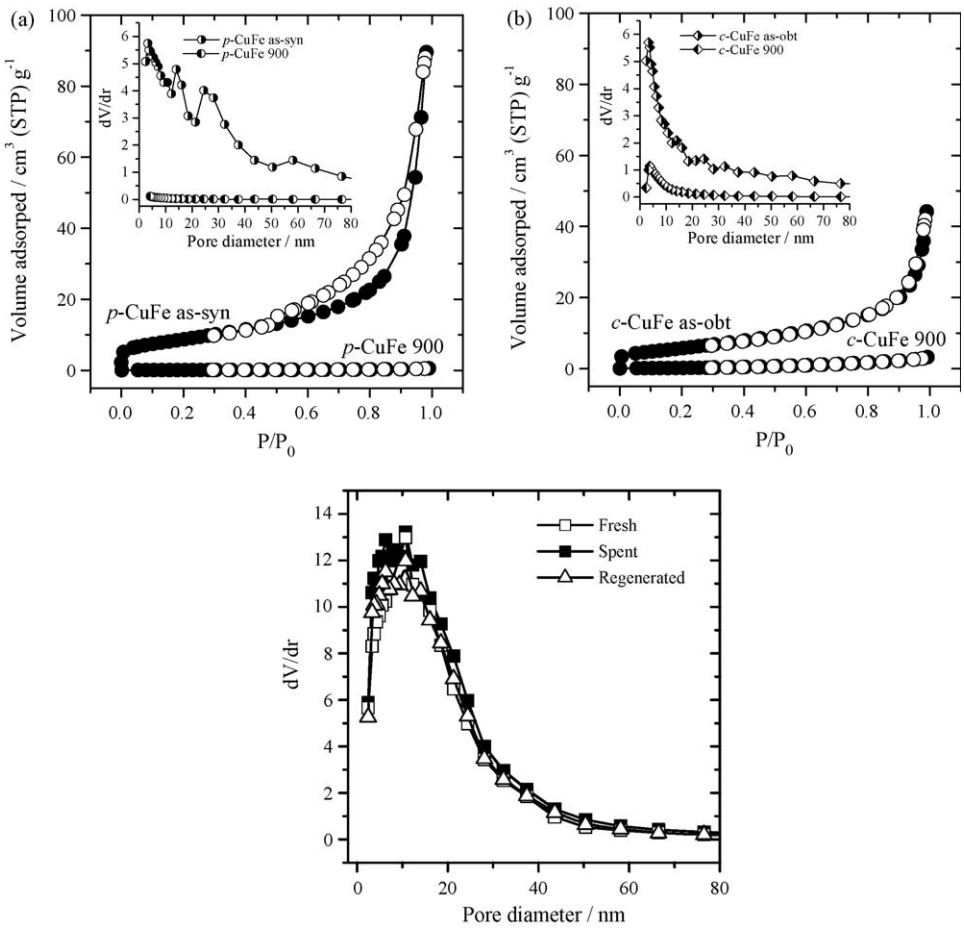

Fig. 11. N_2 adsorption–desorption isotherms and BJH pore size distributions (inset) of (a) *p*-CuFe as-syn, *p*-CuFe 900 and (b) *c*-CuFe as-obt, *c*-CuFe 900 and BJH pore size distributions of (c) fresh, spent, and regenerated composites of *p*-CuFe 900 + Al_2O_3. Reaction conditions: same as in Fig. 6. Regeneration condition: calcination in air at 350 °C for 5 h; adsorption (●), desorption (○).

to the crystal growth and shrinkage of catalyst particles. The decrease in BET surface area from 21.0 to 1.8 $m^2\ g^{-1}$ was also found over the commercial one. The N_2 adsorption–desorption isotherms and the BJH pore size distribution (as an inset) of the spinels are shown in Fig. 11. *p*-CuFe as-syn and *c*-CuFe as-obt showed mesoporous structure with average pore size of 18 and 13 nm, respectively. The pore size distribution of *c*-CuFe as-obt was quite sharp at the size range of 5–15 nm, while that of *p*-CuFe as-syn was broad. The calcined spinels were non-porous with extremely low pore volume below 0.005 ml g^{-1}. The BJH pore size distribution of the fresh, spent, and regenerated catalysts is shown in Fig. 11c. The pore analysis here reflected the change of pore volume in alumina phase, since the pore volume in the spinel phase was relatively negligible. The fresh catalyst has a broad pore size distribution of 5–40 nm with average pore size of 13–14 nm. There are no obvious changes in the pore volume of the fresh, spent, and regenerated catalysts, suggesting that carbon deposition would be insignificant on alumina phase.

We have reported that DME hydrolysis over alumina was very stable, but fast deactivation was observed over ZSM-5 and H-mordenite, especially at high temperatures above 300 °C, due to coking [8]. The formation of carbonaceous species on the composite of CuO/CeO_2 and WO_3/ZrO_2 was suggested to be a main reason of the catalyst deactivation in DME SR [17]. It was also observed that the polymethyl aromatic hydrocarbon was formed on ZSM-5 surface and migrated to Cu surface to form coke during DME SR [19]. The carbonaceous species could be easily formed on acid sites of such strong acid catalysts. In contrast, alumina possesses weak acid sites and would result in less coking [40]. The excellent performance of the spinel-alumina composite catalysts makes it outstanding for an application to fuel cells. For an actual application, a study on catalytic behaviors of the developed catalysts under steady- and unsteady-state operations is under way in our research group.

4. Conclusions

The catalytic performances in DME SR were compared over a series of composite catalysts of γ-Al_2O_3 and $CuFe_2O_4$. The catalysts were characterized by means of XPS, XRD, TPO, TPR, Raman spectroscopy, FTIR, and N_2 adsorption–desorption isotherm. The conclusions based on the present findings are drawn as follows:

1. The $CuFe_2O_4$ spinel in cubic phase was transformed to tetragonal phase by calcining in air at 900 °C. The tetragonal spinel possessed an extremely low BET surface area of 0.5 $m^2\ g^{-1}$ and crystallite size of 45 nm.
2. The *in situ* XPS analysis revealed that the calcined spinel comprised the Cu^{1+}-rich surface after subjected to reduction in 10% H_2/N_2, corresponding to the high catalytic activity in DME SR. The Cu^{1+}/Cu^0 ratio strongly related with the reducibility of Cu species in the spinels. The high dispersion of metallic copper in the matrix of iron oxides reduced from spinel structure and their strong chemical interaction should be attributable to the excellent performance.
3. By increasing S/C ratio, DME conversion could be increased, while CO and CH_4 formations were suppressed. The degradation

rate of the catalyst was also retarded. The carbonaceous deposition was therefore considered as a reason for the gradual degradation of the catalysts. XRD and Raman spectroscopy revealed that the carbon deposition was not in a graphitic form. No evidence for surface formates or carbonates was observed in the FTIR spectra. The size of metallic Cu formed during the DME SR process was ca. 36 nm, and Cu sintering for time-on-stream of 100 h was negligible.

4. The degraded catalysts can be recovered completely by calcination in air at temperatures of 350–800 °C. It turned out that post-reduction treatment in H_2/N_2 at 350 °C was not effective for regeneration of the degraded catalysts.

Acknowledgement

Authors acknowledge the Japan Science and Technology Agency (JST) for financial support. K.F. partially received the financial support from the National Nanotechnology Center and the Thailand Research Fund (TRF).

References

[1] D. Fino, N. Russo, G. Saracco, V. Specchia, J. Catal. 242 (2006) 38.
[2] N. Russo, D. Fino, G. Saracco, V. Specchia, Cat. Today 119 (2007) 228.
[3] K. Sekizawa, S. Yano, K. Eguchi, H. Arai, Appl. Catal. A 169 (1998) 291.
[4] Y. Tanaka, T. Ukata, R. Kikuchi, T. Takeguchi, K. Sasaki, K. Eguchi, J. Catal. 215 (2003) 271.
[5] S. Kameoka, T. Tanabe, A.P. Tsai, Catal. Lett. 100 (2005) 89.
[6] Y. Tanaka, R. Kikuchi, T. Takeguchi, K. Eguchi, Appl. Catal. B 57 (2005) 211.
[7] J. Papavasiliou, G. Avgouropoulos, T. Ioannides, Catal. Commun. 6 (2005) 497.
[8] K. Faungnawakij, Y. Tanaka, N. Shimoda, T. Fukunaga, S. Kawashima, R. Kikuchi, K. Eguchi, Appl. Catal. A 304 (2006) 40.
[9] A.P. Tsai, M. Yoshimura, Appl. Catal. A 214 (2001) 237.
[10] T. Shishido, Y. Yamamoto, H. Morioka, K. Takaki, K. Takehira, Appl. Catal. A 263 (2004) 249.
[11] S. Liu, K. Takahashi, K. Uematsu, M. Ayabe, Appl. Catal. A 283 (2005) 125.
[12] E.S. Ranganathan, S.K. Bej, L.T. Thompson, Appl. Catal. A 289 (2005) 153.
[13] L.C. Wang, Y.M. Liu, M. Chen, Y. Cao, H.Y. He, G.S. Wu, W.L. Dai, K.N. Fan, J. Catal. 246 (2007) 103.
[14] V.V. Galvita, G.L. Semin, V.D. Belyaev, T.M. Yurieva, V.A. Sobyanin, Appl. Catal. A 216 (2001) 85.
[15] K. Takeishi, H. Suzuki, Appl. Catal. A 260 (2004) 111.
[16] T. Mathew, Y. Yamada, A. Ueda, H. Shioyama, T. Kobayashi, Appl. Catal. A 286 (2005) 11.
[17] T. Nishiguchi, K. Oka, T. Matsumoto, H. Kanai, K. Utani, S. Imamura, Appl. Catal. A 301 (2006) 66.
[18] T.A. Semelsberger, K.C. Ott, R.L. Borup, H.L. Greene, Appl. Catal. B 65 (2006) 291.
[19] T. Kawabata, H. Matsuoka, T. Shishido, D. Li, Y. Tian, T. Sano, K. Takehira, Appl. Catal. A 308 (2006) 82.
[20] K. Faungnawakij, Y. Tanaka, N. Shimoda, T. Fukunaga, R. Kikuchi, K. Eguchi, Appl. Catal. B 74 (2007) 144.
[21] K. Faungnawakij, R. Kikuchi, K. Eguchi, Scripta Mater. 60 (2009) 655.
[22] Y. Tanaka, T. Takeguchi, R. Kikuchi, K. Eguchi, Appl. Catal. A 279 (2005) 59.
[23] K. Eguchi, N. Shimoda, K. Faungnawakij, T. Matsui, R. Kikuchi, S. Kawashima, Appl. Catal. B 80 (2008) 156.
[24] K. Faungnawakij, N. Shimoda, T. Fukunaga, R. Kikuchi, K. Eguchi, Appl. Catal. A 341 (2008) 139.
[25] K.H. Wu, C.H. Yu, Y.C. Chang, D.N. Horng, J. Solid State Chem. 177 (2004) 4119.
[26] U. Zavyalova, B. Nigrovski, K. Pollok, F. Langenhorst, B. Müller, P. Scholz, B. Ondruschka, Appl. Catal. B 83 (2008) 221.
[27] S. Rousseau, S. Loridant, P. Delichere, A. Boreave, J.P. Deloume, P. Vernoux, Appl. Catal. B 88 (2009) 438.
[28] E. Santacesaria, S. Carra, Appl. Catal. 5 (1983) 345.
[29] L. Lloyd, D.E. Ridler, M.V. Twigg, in: M.V. Twigg (Ed.), Catalyst Handbook, second ed., Wolfe Publishing, Frome, 1989, p. 283.
[30] J. Hernandez, P. Wrschka, G.S. Oehrlein, J. Electrochem. Soc. 48 (2001) 389.
[31] K. Takahashi, N. Takezawa, H. Kobayashi, Appl. Catal. 2 (1982) 363.
[32] J. Nakamura, T. Uchijima, Y. Kanai, T. Fujitani, Catal. Today 28 (1996) 223.
[33] G.U. Kulkarni, C.N.R. Rao, Top. Catal. 22 (2003) 183.
[34] C.J. Jiang, D.L. Trimm, M.S. Wainwright, Appl. Catal. A 97 (1993) 145.
[35] Y. Choi, S.G. Stenger, Appl. Catal. B 38 (2002) 259.
[36] O. Ilinich, W. Ruettinger, X. Liu, R. Farrauto, J. Catal. 247 (2007) 112.
[37] D.A. Kukuruznyak, J.G. Moyer, N.T. Nguyen, E.A. Sten, F.S. Ohuchi, J. Electron Spectrosc. Rel. Phenom. 150 (2006) 275.
[38] Y. Okamoto, K. Fukino, T. Imanaka, S. Teranishi, J. Phys. Chem. 87 (1983) 3740.
[39] K. Faungnawakij, R. Kikuchi, K. Eguchi, J. Power Sources 164 (2006) 73.
[40] K. Faungnawakij, R. Kikuchi, T. Matsui, T. Fukunaga, K. Eguchi, Appl. Catal. A 333 (2007) 114.